Self-organized nanofibers from a giant nanographene: effect of solvent and deposition method†

Vincenzo Palermo,[a] Susanna Morelli,[a] Christopher Simpson,[b] Klaus Müllen*[b] and Paolo Samorì*[ac]

Received 26th August 2005, Accepted 10th October 2005
First published as an Advance Article on the web 2nd November 2005
DOI: 10.1039/b512137j

We describe the synthesis of the to-date largest soluble nanographene molecule containing 132 carbons in its core and the Scanning Force Microscopy investigation on its self-organization into supramolecular fibers. This alkylated polycyclic aromatic hydrocarbon can grow from solution on solid substrates into fibrils with a length of several micrometers and a cross section of about 16 nm. Making use of different solvents and deposition methods it was possible to achieve a control over the interplay between dewetting and intermolecular π–π stacking, promoting the formation of thermodynamically favoured regular fibrils on mica. On the other hand, under kinetically controlled film growth the formation of ordered supramolecular arrangements at surfaces was hampered. These fibril nanostructures may be useful in the future for the fabrication of molecular nanowires.

Introduction

The development of molecular or supramolecular wires[1] relies on the design of fiber-like structures with an intrinsic electrical conductivity, a notable stiffness and a length of at least some tens of nanometers.[2] Wires having a cross-section on the nanometer scale are required to perform basic electronic operations such as transporting an electric signal. To address this very important issue, different kinds of nanowires have been developed in recent years. The golden candidates are probably carbon nanotubes,[3] although they suffer from difficult purification and separation between species with different conductivities. Other promising alternatives are nanowires of conventional semiconductors[4] and even metals.[5] A different viable approach to grow nanowires relies on supramolecular chemistry as a route to self-organize single molecules into architectures with pre-programmed molecular order and physico-chemical properties.[6] Such a method has already been successfully employed to produce fiber-like architectures from small organic molecules,[7,8] (co-)polymers,[9,10] dendrimers[11] and discotic liquid crystals,[12,13] as recently reviewed.[14] Self-assembly from solution is a simple approach which does not require complex vacuum based methods involving catalysts, such as those needed for the synthesis of carbon or silicon nanotubes. In general, self-assembly at surfaces is governed by the interplay of intramolecular, intermolecular and interfacial interactions.[15,16] A key role influencing the supramolecular organization on a (sub)micrometer scale can be ascribed to the dewetting phenomena during solvent evaporation, the employed deposition method and the concentration of the solution.[17,18]

Polycyclic aromatic hydrocarbons (PAHs) are nanographenes possessing interesting electronic properties.[19,20] The high structural order which can be achieved in the bulk and at surfaces,[12,21–25] along with a large functional electronic component, the PAH core, provide exceptional one-dimensional transport properties,[26] which have been used so far in the development of photovoltaic devices.[27] In particular, the fine tuning of the experimental conditions on a hexa-*peri*-hexabenzocoronene (HBC) made it possible to self-assemble at surfaces structurally defined fibers using a variety of solvents.[28] The use of a PAH larger than HBC provides access to improved electrical properties of supramolecular arrangements, although larger molecules imply also more difficult processability, due to their lower solubility in organic solvents and an onset of decomposition at very high temperatures (>450 °C) required for sublimation in vacuum, and difficult purification.[26]

In this work we focussed our attention on the synthesis and self-assembly of C132-C_{16} (**4**, Scheme 1) on mica. This molecule possesses a central aromatic core which contains 132 aromatic carbon atoms forming a nanoscopic graphene island, and aliphatic C16 (3,7,11,15-tetramethylhexadecyl) side-groups which provide relatively good solubility in some organic solvents. C132-C_{16} forms a liquid-crystalline phase which persists in a wide temperature range from below room temperature to at least 300 °C. In this mesophase the discs are stacked to form columns, with a disc–disc intermolecular distance of 0.35 nm. This distance, which is typical for π–π stacked conjugated discotic molecules, was confirmed by two-dimensional wide-angle X-ray scattering (2D-WAXS).[29] Our effort has been addressed towards the formation of ordered C132-C_{16} anisotropic structures, such as micrometer long regular fibers, by maximizing the effect of intermolecular

[a]*Istituto per la Sintesi Organica e la Fotoreattività, Consiglio Nazionale delle Ricerche, via Gobetti 101, Bologna, I-40129, Italy. E-mail: samori@isof.cnr.it; Fax: +39-051-6399844*
[b]*Max-Planck Institute for Polymer Research, Ackermannweg 10, Mainz, D-55124, Germany. E-mail: muellen@mpip-mainz.mpg.de; Fax: +49-6131-379350*
[c]*Nanochemistry Laboratory, Institut de Science et d'Ingénierie Supramoléculaires (ISIS), Université Louis Pasteur, 8 allée Gaspard Monge, Strasbourg, F-67083, France*
† Electronic supplementary information (ESI) available: experimental procedures; MALDI TOF mass spectra. See DOI: 10.1039/b512137j

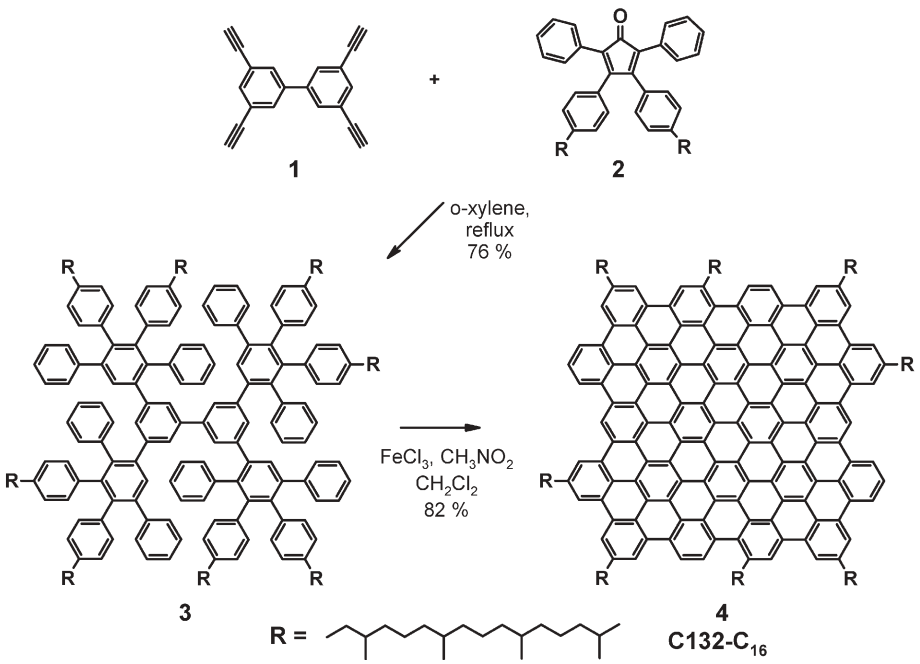

Scheme 1 Synthesis of the octaalkyl C132 PAH **4**.

interactions and minimizing the role of dewetting. This was accomplished by changing the solvent type, the concentration and the solvent evaporation rate. The film morphologies were characterized by Tapping Mode Scanning Force Microscopy (SFM).[30]

Experimental

Details of the experimental procedures undertaken during the synthesis of the compounds as well as the results on the mass spectrometry characterization are given in the ESI.† The C132-C_{16} was dissolved in reagent grade 1,2-dichlorobenzene (DCB) and 1,2,4-trichlorobenzene (TCB). The molecule was processed on freshly cleaved muscovite mica surfaces (Ted Pella Inc.) by either immersion or drop casting. In the former, the whole sample was dipped for 4 min into the solution heated at 160 °C, and then left to dry in air. In the latter, a ~20 μl drop of solution at 160 °C was applied to the mica surface and left to dry in air. Usually the complete solvent evaporation required 1–2 days. The evaporation rate was in some cases decreased by cooling the substrate below room temperature or increased by either exposing the surface to a gentle flow of N_2 or by thermal treatment of the film at 80 °C for 10 min.

After complete solvent evaporation, the morphologies of the dry thin films were explored by means of tapping mode SFM using a Nanoscope IIIa instrument (Veeco, Santa Barbara, CA) operating at room temperature in an air environment. Height and phase images were recorded with microfabricated silicon tips (length 125 μm and width 30 μm) having a spring constant between 17 and 64 N m^{-1}, using scan rates of 1–3 lines s^{-1} and a resolution of 512 × 512 pixels. The measured fiber width w was corrected for tip convolution, using the model proposed in ref. 10: $w_{real} = w_{measured} - 2\sqrt{h(2R-h)}$, where h is the measured height and R is the tip radius, estimated to be ~13 nm.

Results and discussion

Synthesis

In order to push the limits of solubilized PAHs to larger size, a 132 carbon core[31] represented a suitable but challenging candidate. With increasing size, the number of positions where alkyl substituents can be attached to the core does not increase in the same way, so the ratio of carbons in the solubilizing group to those in the rigid core becomes more unfavorable. Whereas smaller PAHs[32] can already be solubilized with dodecyl chains it is therefore necessary in this case to use longer and branched side chains to compensate for this effect and thus make the large molecule soluble and processable.

The synthetic route to the C132-C_{16} compound is depicted in Scheme 1. The tetraphenylcyclopentadienone **2** was reacted with the tetraethynyl biphenyl core **1** under Diels–Alder conditions in boiling *ortho*-xylene to the C132-oligophenylene precursor **3**. The workup of this first generation dendrimer proceeded by evaporation of the solvent, followed by column chromatography to afford a highly viscous, colorless oil in 76% yield.

The cyclodehydrogenation to the C132-C_{16} PAH required the removal of 56 hydrogens or 28 aryl–aryl bond formations in a single reaction step. With increasing size of the desired PAH, the demands for the efficiency of the cyclodehydrogenation reagent rise drastically. The planarization was attempted under oxidative conditions using iron(III) chloride and adapting the time and reagent stoichiometry to the optimum requirements for this specific molecule.[32] It turned out that six equivalents of iron(III) chloride per hydrogen to be removed and four hours reaction time resulted in the best outcome. Upon quenching of the reaction solution, the octaalkyl C132-C_{16} precipitated as a soft, dark purple solid which was collected by filtration and washed thoroughly with methanol

and dilute HCl to remove iron salts. Isotopically resolved mass spectrometry showed the formation of C132-C_{16} as a monodisperse and highly pure compound (see ESI†).

In spite of its solubility, NMR spectroscopy showed no resolved signals of C132-C_{16} in the aromatic region. This meant that the burden of structure proof for this giant PAH lay mainly on mass spectrometry which is (so far) generally not regarded as an adequate method on its own. It has to be pointed out however that the possibility of isotopic resolution of such a high molecular weight compound enables the exact comparison of the measured spectrum with the calculated isotopic distribution for $C_{292}H_{354}$, which stretches already over nine mass units. There is no other structure than the proposed one for C132-C_{16} thinkable which would fit exactly to the calculated spectrum. Furthermore it was shown previously that partially cyclized and dendritic precursor structures are exaggerated due to their lower desorption energy if they are present.[33,34] Therefore the mass spectrum can be regarded as proof not only of the structure of the to date largest alkyl substituted and soluble PAH C132-C_{16} but also of its high purity.

Scanning force microscopy (SFM)

C132-C_{16} exhibits low solubility in several organic solvents, which is caused by the large size of its conjugated core and its consequent tendency to form clusters in solution. Among the different solvents conventionally used for polyaromatic compounds, 1,2-dichlorobenzene (DCB) was first chosen because it could relatively well dissolve C132-C_{16} (**4**). Fig. 1a-c shows the SFM images of films of C132-C_{16} prepared by immersion of mica in C132-C_{16} solutions in DCB at various concentrations. The film grown from a concentrated solution, *i.e.* 10^{-5} mol l^{-1}, reveals a layer architecture exposing circular holes (Fig. 1a). The height of the layer, as determined from topographical profiles, is ~3 nm. Such a size is similar to the molecular diameter, which amounts to about 2.2 nm if one considers just the rigid aromatic core. Upon dilution of the solution (10^{-6} mol l^{-1}) the holes in the layer expanded and coalesced, leading to the formation of a discontinuous network (Fig. 1b). Fig. 1c displays a film prepared with a lower concentration (10^{-7} mol l^{-1}); it exhibits a surface covered with globular isolated aggregates, some of them having an anisotropic shape. Films prepared from even more diluted solutions produce rounded droplets (image not shown). It is therefore important to point out that we were not able to form fibers from C132-C_{16} solutions in DCB. The trend in the morphologies as a function of the concentration shown in Fig. 1a–c needs to be compared with a model proposed recently to describe drying-mediated self-assembly of nanoparticles solutions.[18] According to this model, the solvent evaporation proceeds through the formation of circular solution-free areas on the substrate which enlarge and eventually coalesce. The obtained nanoparticle arrangement depends on the solvent evaporation rate and nanoparticle diffusion into the solution. If evaporation is uniform, a continuous layer is produced. On the other hand, less uniform evaporation leads to the formation of circular holes in the layer which are similar to those shown in Fig. 1a. If these holes have the possibility to enlarge further and coalesce, a broken network similar to Fig. 1b is obtained (see for comparison Fig. 4b of ref. 18). The stability of a molecular domain at surfaces depends on its interfacial energy, therefore it is proportional to its area/circumference ratio.[35,36] Such a ratio, which corresponds to the aspect ratio, for the network of Fig. 1b is very small since it has a very long perimeter. The interaction of the molecules at domain boundaries with the solvent can induce a molecular rearrangement that emerges as a disruption of the network, and consequent formation of irregular branched clusters such as those shown in Fig. 1c. In an infinite time the process yields isolated rounded droplets. The good agreement between the Rabani model and the results shown in Fig. 1a–c suggests that the surface morphology of C132-C_{16} is strongly influenced by dewetting, due to solvent evaporation.[18]

A reduction of the dewetting contribution to the self-organization of the molecules at surfaces can be achieved by decreasing the rate of solvent evaporation.[28,37] This can be accomplished either using a low volatility solvent or preparing the film in a sealed atmosphere saturated by the vapours of the solvent. We have therefore extended the studies to films prepared using a different solvent such TCB which is similar to DCB but possesses both lower volatility, due to a boiling temperature of 213 °C *vs.* 180 °C for DCB, and different polarity, due to the presence of one additional chlorine atom.[38]

Fig. 2a shows the morphology of a film prepared from immersion in a 5×10^{-7} mol l^{-1} solution in TCB. The SFM image reveals some isolated fibers and irregular isotropic-shaped agglomerates coexisting on the mica surface. The fiber exhibits a height of ~4.5 nm, a width of ~40 nm and a length of more than 10 μm. The isotropic-shaped agglomerates have a lateral size ranging from 100 to 500 nm and heights of some

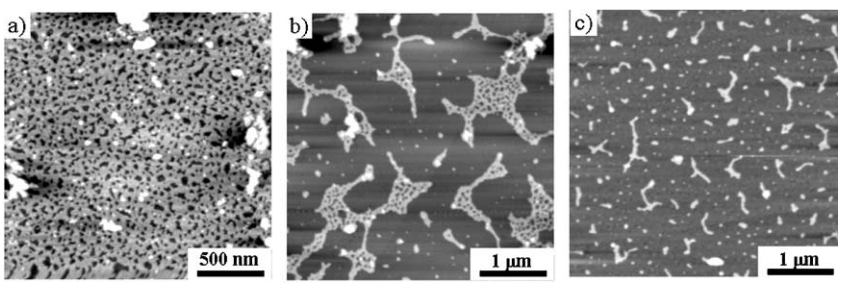

Fig. 1 SFM topographical images of C132-C_{16} deposited on mica by immersion in DCB solutions at concentrations of (a) 10^{-5} mol l^{-1}, (b) 10^{-6} mol l^{-1}, (c) 10^{-7} mol l^{-1}. Z-scales are (a) 5.5 nm, (b) 9 nm and (c) 6.5 nm.

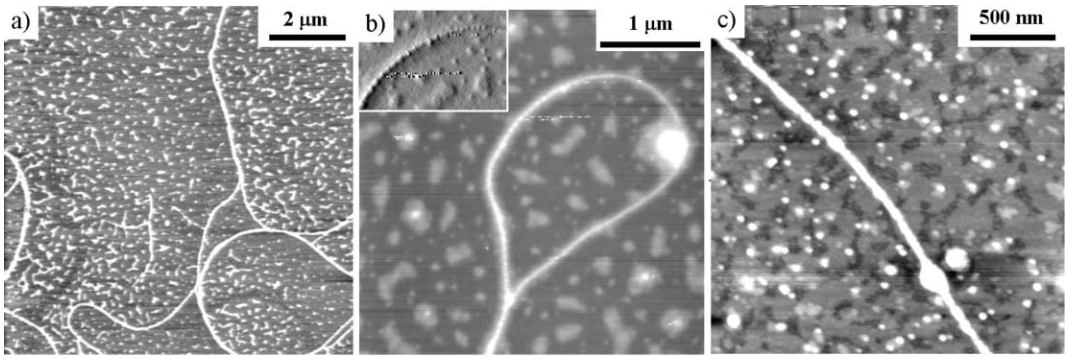

Fig. 2 SFM topographical images of a film of (a) C132-C_{16} molecules arranged in supramolecular fibers, obtained by immersion in a TCB solution at 5×10^{-7} mol l^{-1}; (b) zoom-in on a fiber forming a lace. In the inset, a detail of the fiber has been gradient-filtered, to show the periodical pattern; (c) single fiber lying on a C132-C_{16} layer, obtained by drop casting a 10^{-8} mol l^{-1} solution in TCB. Z-scales are (a) 6 nm, (b) 17 nm and (c) 4.5 nm.

nanometers. The difference in film morphology obtained using DCB and TCB indicates that both the lower polarity and volatility play important roles in the self-organization at surfaces. An important contribution can be ascribed also to the different viscosity of the solvent.

The isotropic-shaped agglomerates at surfaces coexisting with fibers in the C132-C_{16} film shown in Fig. 2a are similar to those obtained with DCB (Fig. 1c). This provides evidence for the important role still played by dewetting. The fibers are usually bent and entangled, forming in some cases complex knots and laces (shown as an example in Fig. 2b). In particular, although the resolution attained does not allow the fine structure of these fibers to be resolved, it appears that they possess a periodic contrast along their contour, with a periodicity ranging from 50 to 90 nm (see inset). This effect might be ascribed to fiber supercoiling leading to a helical superstructure. Despite the known tendency of C132-C_{16} to arrange into columnar structures in the mesophase,[26] the low density of the observed fibers demonstrates that the dewetting still partially hinders the formation of ordered structures at surfaces.

In order to cast light onto the role of the deposition method on the self-assembly at surfaces we prepared a new set of samples changing the sample preparation method, namely using drop-casting instead of immersion. In drop-casting a single drop of liquid is applied to the surface; the solvent evaporation tends to proceed from the drop edges towards the center leading to an inhomogeneous coating of the substrate. Also here a low density of fibers was obtained, having an average length of several micrometers, a width of $\sim$52 nm and a height of $\sim$4 nm. These fibers are adsorbed on a thin discontinuous layer possessing a thickness of $\sim$1 nm and which is itself partially covered by rounded clusters with a height of $\sim$3 nm (Fig. 2c). The smaller thickness of the layer of Fig. 2c when compared to the one shown in Fig. 1a might be explained in view of a different orientation of the molecule on the substrate. This confirms the important role played by the solvent in the molecular arrangement on surfaces.

In both methods employed for the film preparation, namely immersion and drop-casting, the dynamics of solvent evaporation from the surface is a complex process. In particular for drop-cast films the degree of coverage in the central area of the sample is usually higher due to the receding drop during solvent evaporation. For the fibers obtained by drop-casting, most of the sample surface was quite irregular, due to the inherent heterogeneity of the deposition method. Unfortunately, we have not been able to grow well-ordered molecular aggregates with a fast deposition method such as spin-coating, even using low spinning rates. This can also be ascribed probably to both the absence of a nucleation occurring from a supernatant solution and to the scarce amount of material left on the surface as a consequence of the centrifugal force.

Aiming at increasing the yield of fibers formed on the surface, attempts were made to further slow down the evaporation speed and reduce in this way the effect of dewetting. Samples were kept at low temperatures (4 °C) for very long times, *i.e.* 4–8 days. Unfortunately this method was not successful, as very few fibers were formed on the surface. Moreover it was found to be impractical because of the long time needed to remove the solvent.

In order to accelerate the drying process, the sample was prepared on a substrate at 4 °C and right after the solution deposition it was heated slowly to room temperature, for about 5 hours. The SFM image of the film obtained following such procedure from a 10^{-6} mol l^{-1} solution in TCB is shown

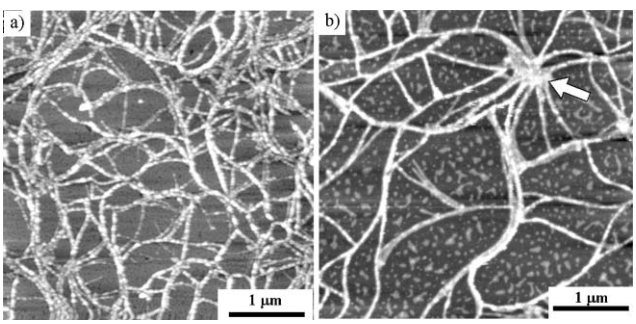

Fig. 3 SFM topographical images of the C132-C_{16} fibers obtained by drop casting a solution in TCB, on a cold mica surface (see text for details): (a) from a 10^{-6} mol l^{-1} solution, (b) from a 5×10^{-7} mol l^{-1} solution. In (b) the solvent evaporation has been accelerated by fluxing a gentle flow of N_2 after 3 hours from the drop deposition. Z-scales are (a) 10 nm and (b) 9 nm.

in Fig. 3a. The image exhibits a surface homogeneously covered by bundles of fibers with lengths >10 μm, width ~21 nm, and height ~5.3 nm. In order to understand if the final molecular arrangement is mainly governed by the self-assembly occurring in the first few hours after the solution deposition, another set of samples were dried with a gentle flow of N_2 three hours after the drop deposition. The typical morphology of this type of film is shown in Fig. 3b. It shows shape persistent fibers with lengths >10 μm, width 16 nm and height 12 nm. In Fig. 3a, the fibers exhibit a surface that seems to be covered by small grains not periodically distanced, packed head-to-tail forming the fibers. In Fig. 3b the fiber cross-section appears more uniform, their density slightly smaller and their dimension larger compared to Fig. 3a.

The complex bundled structures observed in Fig. 2a and b together with the well known tendency of C132-C_{16} to aggregate in solution and form columnar structures in the mesophase suggest that at least small fibers segments start forming in solutions. This is in particular confirmed by the three-dimensional character of the fiber-lace in Fig. 2b. Upon deposition at surface they can pack head-to-tail leading to micrometer long fibers. When the liquid layer reaches a critical thickness dewetting occurs according to the process described previously,[18,39] causing the pulling of the fibers along the receding lines of the drop. The ratio between the thermodynamically favoured fibers and the kinetically driven irregular agglomerates due to the dewetting process can be modulated by varying the experimental conditions. If the temperature is too high or the solvent too volatile, dewetting shear forces are predominant, and a disordered pattern is obtained. However, if one chooses a suitable solvent, deposition method and temperature, the dewetting contribution to self-organization is minimized, favouring the formation of fibers. The critical time frame for fiber formation seems to be in the first hours after deposition, which is very likely to be characterized by a higher molecular dynamics allowing reorganization due to the solvent layer still present on the surface. The result shown in Fig. 3b unambiguously reveals that three hours after the deposition the fibers are formed at surfaces. Their stability is pretty high since they could not be disrupted even under the effect of N_2 flux or high temperature treatments. If instead N_2 fluxing or heating were performed just after the application of the drop to the surface, a disordered pattern was obtained.

Although under the conditions used to prepare the film of Fig. 3b the dewetting does not hamper the fiber generation, in some cases it can drive the supercoiling of fibers in given locations, leading to the formation of star-shaped bundles (white arrow in Fig. 3b). This clustering of fibers has already been observed for similar systems, and is further evidence of the shear forces due to dewetting, which "pull" the fibers concentrating them in the areas where the solvent lasts longer during evaporation.[37] Suppression of the contribution of dewetting governing the formation of the patterns shown in Fig. 1a–c was attained by tuning the self-assembly kinetics, which required a proper choice of the solvent and processing temperature. Under these conditions the molecules are prone to self-assemble in the thermodynamically favoured arrangement. The kinetics of the self-organization was found to be a key factor governing the formation of ordered dry supramolecular architectures from conjugated (macro)molecules at surfaces.[40,41] The thicknesses of the supramolecular architectures observed in this work suggest a molecular packing characterized by π–π stacks with the molecular discs preferentially arranged "edge-on" on the basal plane of the surface eventually forming long fibers. This is in good agreement with the well-known tendency of conjugated molecules bearing aliphatic side-groups to pack "edge-on" on the basal plane of the insulating mica surface, also because of the different hydrophobic and hydrophilic characters of the admolecule and of the substrate, respectively.[10]

Conclusions

We have shown the successful synthesis of the C132-C_{16} PAH as a soluble and thereby processable material with the ability to form ordered supramolecular structures. By varying systematically different experimental conditions it is possible to drive the self-assembly of C132-C_{16} at surfaces towards well organised supramolecular fibrils. We have focussed on the competition between the dewetting process taking place during the solvent evaporation and the intermolecular interactions, in particular π–π stacking. While the former was found to hinder the formation of ordered architectures, the latter turned out to promote the self-assembly towards very long fibrils with a constant cross section. The maximization of the degree of order within the film was achieved making use of a solvent possessing a high boiling point and a relatively low polarity. The minimization of the role of dewetting and maximization of the contribution of intermolecular interaction was accomplished by varying the solvent evaporation rate during the film preparation, favouring the self-organization into fibers. Although the complete removal of the solvent required a few days due to their high boiling points, the key time frame for the fiber formation was found to be the first hours after the application of the drop to the substrate. The great importance of using a slow rate of solvent evaporation favouring therefore the crystallization process indicates that the growth of these nanostructures is a kinetically governed phenomenon. The fiber supramolecular assemblies might be good candidates to be used in the future as molecular nanowires in molecular scale electronic devices.

Acknowledgements

We thank Matteo Palma and Anna Maria Talarico for enlightening discussions. Financial support from ESF-SONS-BIONICS, the EU through the Integrated Project NAIMO (NMP4-CT-2004-500355), the Marie Curie EST project SUPER (MEST-CT-2004-008128), the ForceTool project (NMP4-CT-2004-013684) as well as from the bilateral project CNR-CNRS is gratefully acknowledged.

References

1 A. Nitzan and M. A. Ratner, *Science*, 2003, **300**, 1384.
2 P. Samorì, H. Engelkamp, P. A. J. de Witte, A. E. Rowan, R. J. M. Nolte and J. P. Rabe, *Adv. Mater.*, 2005, **17**, 1265.

3 A. Bachtold, P. Hadley, T. Nakanishi and C. Dekker, *Science*, 2001, **294**, 1317.
4 S. P. Ge, K. L. Jiang, X. X. Lu, Y. F. Chen, R. M. Wang and S. S. Fan, *Adv. Mater.*, 2005, **17**, 56.
5 Y. Wu, J. Xiang, C. Yang, W. Lu and C. M. Lieber, *Nature*, 2004, **430**, 61.
6 Special issue on Supramolecular chemistry and self-assembly, *Science*, 2002.
7 A. Schenning, A. F. M. Kilbinger, F. Biscarini, M. Cavallini, H. J. Cooper, P. J. Derrick, W. J. Feast, R. Lazzaroni, P. Leclère, L. A. McDonell, E. W. Meijer and S. C. J. Meskers, *J. Am. Chem. Soc.*, 2002, **124**, 1269.
8 J. M. Xu, C. Z. Zhou, L. H. Yang, N. T. S. Chung and Z. K. Chen, *Langmuir*, 2004, **20**, 950.
9 P. Leclère, A. Calderone, D. Marsitzky, V. Francke, Y. Geerts, K. Müllen, J. L. Brédas and R. Lazzaroni, *Adv. Mater.*, 2000, **12**, 1042.
10 P. Samorì, V. Francke, K. Müllen and J. P. Rabe, *Chem. Eur. J.*, 1999, **5**, 2312.
11 D. J. Liu, H. Zhang, P. C. M. Grim, S. De Feyter, U. M. Wiesler, A. J. Berresheim, K. Müllen and F. C. De Schryver, *Langmuir*, 2002, **18**, 2385.
12 A. M. van de Craats, N. Stutzmann, O. Bunk, M. M. Nielsen, M. Watson, K. Müllen, H. D. Chanzy, H. Sirringhaus and R. H. Friend, *Adv. Mater.*, 2003, **15**, 495.
13 A. S. Drager, R. A. P. Zangmeister, N. R. Armstrong and D. F. O'Brien, *J. Am. Chem. Soc.*, 2001, **123**, 3595.
14 F. J. M. Hoeben, P. Jonkheijm, E. W. Meijer and A. P. H. J. Schenning, *Chem. Rev.*, 2005, **105**, 1491.
15 J. P. Rabe and S. Buchholz, *Science*, 1991, **253**, 424.
16 P. Samorì, N. Severin, K. Müllen and J. P. Rabe, *Adv. Mater.*, 2000, **12**, 579.
17 V. Palermo, M. Palma, Z. Tomovic, M. D. Watson, K. Müllen and P. Samorì, *Synth. Met.*, 2004, **147**, 117.
18 E. Rabani, D. R. Reichman, P. L. Geissler and L. E. Brus, *Nature*, 2003, **426**, 271.
19 M. D. Watson, A. Fechtenkötter and K. Müllen, *Chem. Rev.*, 2001, **101**, 1267.
20 F. Jäckel, M. D. Watson, K. Müllen and J. P. Rabe, *Phys. Rev. Lett.*, **2004**, 92.
21 P. Samorì, A. Fechtenkötter, F. Jäckel, T. Böhme, K. Müllen and J. P. Rabe, *J. Am. Chem. Soc.*, 2001, **123**, 11462.
22 P. Samorì, N. Severin, C. D. Simpson, K. Müllen and J. P. Rabe, *J. Am. Chem. Soc.*, 2002, **124**, 9454.
23 R. Friedlein, X. Crispin, C. D. Simpson, M. D. Watson, F. Jäckel, W. Osikowicz, S. Marciniak, M. P. de Jong, P. Samorì, S. K. M. Jonsson, M. Fahlman, K. Müllen, J. P. Rabe and W. R. Salaneck, *Phys. Rev. B*, 2003, **68**, 195414.
24 J. S. Wu, M. D. Watson, L. Zhang, Z. H. Wang and K. Müllen, *J. Am. Chem. Soc.*, 2004, **126**, 177.
25 P. Samorì, X. M. Yin, N. Tchebotareva, Z. H. Wang, T. Pakula, F. Jäckel, M. D. Watson, A. Venturini, K. Müllen and J. P. Rabe, *J. Am. Chem. Soc.*, 2004, **126**, 3567.
26 M. G. Debije, J. Piris, M. P. de Haas, J. M. Warman, Z. Tomovic, C. D. Simpson, M. D. Watson and K. Müllen, *J. Am. Chem. Soc.*, 2004, **126**, 4641.
27 L. Schmidt-Mende, A. Fechtenkötter, K. Müllen, E. Moons, R. H. Friend and J. D. MacKenzie, *Science*, 2001, **293**, 1119.
28 M. Kastler, W. Pisula, D. Wasserfallen, T. Pakula and K. Müllen, *J. Am. Chem. Soc.*, 2005, **127**, 4286.
29 C. D. Simpson, J. S. Wu, M. D. Watson and K. Müllen, *J. Mater. Chem.*, 2004, **14**, 494.
30 P. Samorì, *Chem. Soc. Rev.*, 2005, **34**, 551.
31 F. Morgenroth, E. Reuther and K. Müllen, *Angew. Chem., Int. Ed. Engl.*, 1997, **36**, 63.
32 A. Fechtenkötter, N. Tchebotareva, M. Watson and K. Müllen, *Tetrahedron*, 2001, **57**, 3769.
33 C. D. Simpson, J. D. Brand, A. J. Berresheim, L. Przybilla, H. J. Räder and K. Müllen, *Chem. Eur. J.*, 2002, **8**, 1424.
34 L. Przybilla, J. D. Brand, K. Yoshimura, H. J. Rader and K. Müllen, *Anal. Chem.*, 2000, **72**, 4591.
35 A. Stabel, R. Heinz, F. C. De Schryver and J. P. Rabe, *J. Phys. Chem.*, 1995, **99**, 505.
36 P. Samorì, K. Müllen and H. P. Rabe, *Adv. Mater.*, 2004, **16**, 1761.
37 D. J. Liu, S. De Feyter, M. Cotlet, U. M. Wiesler, T. Weil, A. Herrmann, K. Müllen and F. C. De Schryver, *Macromolecules*, 2003, **36**, 8489.
38 The dielectric constants of TCB and DCB amount to 2.24 and 9.93, respectively.
39 S. Herminghaus, K. Jacobs, K. Mecke, J. Bischof, A. Fery, M. Ibn-Elhaj and S. Schlagowski, *Science*, 1998, **282**, 916.
40 P. Samorì, M. Keil, R. Friedlein, J. Birgerson, M. Watson, M. Müllen, W. R. Salaneck and J. P. Rabe, *J. Phys. Chem. B*, 2001, **105**, 11114.
41 P. Samorì, V. Francke, K. Müllen and J. P. Rabe, *Thin Solid Films*, 1998, **336**, 13.